Accepted version
https://doi.org/10.1016/j.saa.2022.121010

Spectroscopic investigation on 1,2-substituted ferrocenes with only planar chirality: how chiroptical data are related to absolute configuration and to substituents

Giuseppe Mazzeo,[a] Sonia Pedotti,[b] Giovanna Longhi,[a,c]
Angela Patti,[*b] Sergio Abbate[*a,c]

[a]*Dipartimento di Medicina Molecolare e Traslazionale (DMMT), Universita` di Brescia, Viale Europa 11, 25123 Brescia, Italy.*

[b]*Institute of Biomolecular Chemistry – CNR, Via Paolo Gaifami 18, 95126 Catania, Italy.*

[c]*INO-CNR, Sede Secondaria di Brescia, via Branze, 45 - 25123 Brescia, Italy*

[*]Corresponding author. E-mail: sergio.abbate@unibs.it; angela.patti@cnr.it

ABSTRACT: Single enantiomers of three 1,2-substituted ferrocene derivatives, *i.e.* 1-methoxymethyl-2-hydroxymethylferrocene (**1**), 1-formyl-2-hydroxymethylferrocene (**2**) and 1-iodo-2-hydroxymethylferrocene (**3**), sharing the common hydroxymethyl substituent and the presence of planar chirality only, were investigated for their spectroscopic (IR and UV) and chiroptical (VCD and ECD) properties. Both enantiomers of **1** were obtained for the first time in optically pure form by lipase-catalyzed kinetic resolution of the corresponding racemate (±)-**1** and separately converted into formyl derivatives (+)-**2** and (–)-**2**.
The experimental spectroscopic and chiroptical data were compared with DFT calculated spectra and excellent correspondence was found for all compounds, allowing one to confirm the previously assigned absolute configurations. The common features in the VCD spectra of a doublet between 940 and 965 cm^{-1} and the short-wavelength (about 200 nm) doublet and the longest wavelength band in the ECD spectra were analyzed to test whether they may be taken as markers of the absolute configuration (AC). The predominance of conformers with intramolecular hydrogen bond for the first two investigated compounds is predicted by conformational analysis and also confirmed by NMR.

KEYWORDS: Ferrocenes; Planar Chirality; Lipase-catalyzed resolution; VCD and ECD spectroscopies; Density Functional Theory (DFT) calculations; Hydrogen Bonding (HB)

1. Introduction

Ferrocene is the most investigated example of metallocene for its peculiar physical features and chemical reactivity, stability and redox-reversibility. Ferrocene derivatives have attracted continuously growing interest in different fields and they find main applications in catalysis,

material science, electrochemistry and medicinal chemistry [1-6]. Chiral ferrocenes are also known, for most of which chirality is due to the presence of stereogenic carbon(s) in the side chain substituent, whereas planar chirality arises when two different substituents are present on the same cyclopentadienyl ring.

The chiroptical analysis of chiral ferrocenes has been usually carried out by electronic circular dichroism (ECD), which has been applied to ferrocene-peptide conjugates [7-8], complexes with cyclodextrins [9], ferrocene-labeled polymers [10-11] and some planar chiral derivatives [12-13], whereas vibrational circular dichroism (VCD has been recently employed also on a few mono-substituted ferrocenes bearing chiral pendants [7,14] and a series of 1,2-disubstituted ferrocenes bearing an additional chiral group in the side chain [15].

The potential of the ferrocene chromophore as a CD probe as well as electrochemically switchable VCD amplifier has been recently evidenced [16], but deep investigation of the basic chiroptical features of ferrocene derivatives and the associated configurational/conformational aspects is quite limited. In order to increase the knowledge on the role of chirality for substituted ferrocenes, in this work we consider the 1,2-disubstituted derivatives **1**, **2** and **3** (1-methoxymethyl-2-hydroxymethylferrocene, 1-formyl-2-hydroxymethylferrocene and 1-iodo-2-hydroxymethyl-ferrocene, respectively), which have the hydroxymethyl substituent in common (Scheme 1), as examples of ferrocenes with planar chirality only.

To the best of our knowledge, this class of ferrocene derivatives has not yet been investigated by chiroptical methods, so both ECD and VCD techniques were applied to the single enantiomers of **1**-**3** and the obtained data were compared with the results from density functional theory (DFT) calculations.

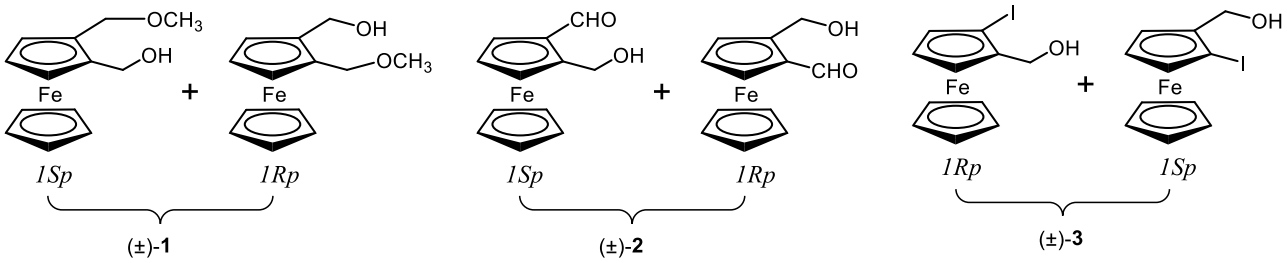

Scheme 1. Structures of the investigated compounds (configuration specification according to ref. [17])

The obtained results proved that both chiroptical techniques are quite sensitive in easily and safely assigning the absolute configuration (AC) of the two enantiomers of (±)-**1**, (±)-**2** and (±)-**3**. The AC of single enantiomers of (±)-**2** and (±)-**3** had been previously assigned [18, 19], while for (+)-**1** and (–)-**1** the AC is assigned in the course of the present study by chemical correlation

methods (*vide infra*) and for all the molecules the chiroptical methods discussed here allowed us to assess and substantiate the conclusions reached independently.

Additionally, we were interested in assessing the role and relative importance of the hydrogen bond (HB) on chiroptical responses, as a continuation of our previous study in which some attention was paid at the phenomena related to the presence of a hydroxyl group and its ability to interact with vicinal groups [14]. In both **1** and **2** the -CH_2OH is able to entertain hydrogen bond with neighboring groups, i.e. the aldehyde or the methoxy group, with the pentadienyl ring or even the iron itself and we aimed to better clarify if and how the conformational properties associated with some HB or other interactions have consequences on the chiroptical response under study.

On the other hand, investigation of known compound (±)-**3** [19] is expected to illustrate a different situation, where either non-existent or very weak intramolecular HB is predictable between OH and I. The critical data to monitor the HB effect include the OH, the C=O and C-O stretching regions in VCD spectra and the far-UV and visible/near UV (Vis) regions in the ECD spectra; concurrently we tried to assess the robustness of the corresponding VCD or ECD signals in the assignment of AC, also with the support of solvent-dependent theoretical investigations.

2. Materials and methods

2.1. General.

^1H and ^{13}C NMR spectra were recorded at 400.13 and 100.62 MHz, respectively, in $CDCl_3$. Chemical shifts (δ) are given as ppm relative to the residual solvent peak and coupling constants (*J*) are in Hz. In the NMR assignment Cp and Cp' refers to substituted and unsubstituted cyclopentadienyl ring, respectively. HPLC analyses were carried out on a Dionex instrument equipped with an Ultimate 3000 high-pressure binary pump, an ASI-100 autosampler, a TCC-100 thermostated column compartment and a UVD-100 multiple wavelength detector set at 210, 230 and 250 and 280 nm. A Phenomenex Lux® 5μm cellulose-2 column was used, eluting with *n*-hexane/2-PrOH mixtures as a mobile phase at flow 0.5 mL/min.

Optical rotations (OR) were measured on a DIP 135 JASCO instrument using a 10 cm length cell.

Lipase from *Candida rugosa*, Amano lipase PS (immobilized on diatomite, PSL-D), Amano lipase AK from *Pseudomonas fluorescens*, Novozym® (immobilized lipase from *Candida Antarctica*) and Lipozyme® (immobilized lipase from *Mucor miehei*) were purchased from Sigma-Aldrich. Lipase immobilized on ceramic particles from *Pseudomonas cepacia* (PSL-C) was from

Fluka. Working conditions and performances are provided in Table SI-1 (S1 of Supplementary Material)

All chemicals were used as received. Deactivated silica gel was obtained by suspending silica gel in *n*-hexane/triethylamine (95:5) and stirring for 30 min., then the solvent was removed by vacuum filtration and the powder dried under a stream of nitrogen. After suspension of the powder in the suitable eluent, the obtained silica gel was used for packing chromatographic column.

1-Formyl-2-methoxymethylferrocene (±)-**4** was prepared from 1-methoxymethylferrocene according a reported procedure [20].

*2.2. Synthesis of 1-hydroxymethyl-2-methoxymethylferrocene (±)-**1**.*

Aldehyde (±)-**4** (600 mg, 2.32 mmol) was dissolved in THF/MeOH (5:1 v/v, 20 mL) and $NaBH_4$ (100 mg, 2.64 mmol) was added. The reaction mixture was stirred at room temperature for 30 min, then diluted with water and extracted with CH_2Cl_2 (3 × 10 ml). Collected organic layers were washed with brine and dried over Na_2SO_4. The solvent was then removed under vacuum at 40°C to give (±)-**1** (590 mg, 2.27 mmol, 98% yield) as a yellow oil, which was used without further purification. ^{1}H-NMR: δ 2.66 (br s, 1H, -OH), 3.34 (s, 3H, -OCH_3), 4.08 (s, 1H, Cp), 4.11 (s, 5H. Cp'), 4.24 (m, 3H, 2 × CH_a-O and Cp), 4.57 (m, 2H, 2 × CH_b-O). ^{13}C-NMR: δ 57.9 (CH_3-O), 59.6 (-CH_2OH), 66.8 (-*C*H_2OCH_3), 68.8 (Cp'), 69.7 (Cp), 69.9 (Cp), 70.5 (Cp), 82.4 (Cp-q), 87.6 (Cp-q). HR-ESI-MS: 260.0535 $[M]^+$, 283.0435 $[M+Na]^+$. Theor. for $C_{13}H_{16}FeO_2$ 260.0500.

*2.3. Preparation of (+)-**1** and (–)-**1** by a sequence of lipase-catalyzed esterification reactions*

To a solution of alcohol (±)-**1** (590 mg, 2.27 mmol) in *n*-hexane (30 mL) immobilized lipase from *P. cepacia* (PsL-D, 1g) and vinyl acetate (0.6 mL, 560 mg, 6.51 mmol) were added and the suspension was stirred in a rotary shaker at 300 rpm and 28 °C for 15 h when 68% of the substrate conversion was reached. After filtration of the enzyme, the solution was taken to dryness and the residue purified on a deactivated silica gel column (*n*-hexane:AcOEt 7:3) to give ($1R_p$)-1-acetoxymethyl-2-methoxymethylferrocene (–)-**5** (440 mg, 1.46 mmol, 64% yield, 44% *ee*) and unreacted *($1R_p$)-1-methoxymethyl-2-hydroxymethyl-ferrocene* (+)-**1** (177 mg, 0.68 mmol, 30% yield, 94% *ee*) as orange oils. *($1R_p$)-1-methoxymethyl-2-hydroxymethylferrocene* (+)-**1**: $[\alpha]_D^{25}$ +14.2 (*c* 0.27, $CHCl_3$ 94% *ee*). HPLC: *n*-hexane:2-PrOH 85:15, t_R/min: 25.01 ($1S_p$) and 38.53 ($1R_p$).

Acetate (–)-**5** (177 mg, 0.68 mmol, 30% yield, 94% *ee*) was dissolved in CH_3CN/H_2O (10:1 v/v 20 mL) and the solution stirred at room temperature for 24 h. The solvent was then removed under reduced pressure to give (–) **1** (360 mg, 1.38 mmol, 95 % yield, 44% *ee*) which was used without further purification.

Scalemic alcohol (–)-**1** (360 mg, 1.38 mmol, 44% *ee*) was dissolved in *n*-hexane (20 ml) and to this solution vinyl acetate (320 μL, 340 mg, 3.95 mmol) and PsL-D lipase (0.8 g) were added. The suspension was shaken at 300 rpm and 28°C, monitoring the reaction course by HPLC. After 3 hours the reaction was stopped by filtering off the enzyme, and the solvent evaporated under vacuum. The residue was purified by flash chromatography on deactivated silica gel using *n*-hexane:AcOEt (7:3 v/v) to give (–)-**5** (250 mg, 0.83 mmol, 60% yield, 91% *ee*) and (+)-**1** (125 mg, 0.48 mmol, 35% yield, 33% *ee*). *(1R_p)-1-acetoxymethyl-2-methoxymethylferrocene* (–)-**5**: $[\alpha]_D^{25}$ – 8.5 (*c* 0.50, $CHCl_3$); ^{1}H-NMR: δ 2.05 (s, 3H, -$COOCH_3$), 3.32 (s, 3H, -OCH_3), 4.13 (s, 5H, Cp'), 4.19 (m, 2H, -CH_a-O and Cp), 4.30 (m, 3H, -CH_b-O and 2 × Cp), 4.91 and 5.03 (d, 1H each, AB system, *J* = 12.4 Hz); ^{13}C-NMR: δ 20.9 (*C*H_3CO-), 57.9 (CH_3-O), 60.9 (*C*H_2-OCO), 67.9 (*C*H_2-O-CH_3), 68.8 (Cp), 69.0 (Cp'and Cp), 70.7 (Cp), 80.9 (Cp-q), 83.4 (Cp-q), 170.8 (-CO). Enantiomeric excess of (–)-**5** was measured after hydrolysis to the corresponding alcohol (–)-**1**. HR-ESI-MS: 302.0647 $[M]^+$, theor. for $C_{15}H_{18}FeO_3$ 302.0605.

Acetate (–)-**5** (250 mg, 0.83 mmol, 91% *ee*) was dissolved in CH_3CN/H_2O (10:1 v/v 20 mL) and the solution stirred at room temperature for 24 h. The solvent was then removed under reduced pressure to give *(1S_p)-1- methoxymethyl-2-hydroxymethylferrocene* (–) **1** (205 mg, 0.79 mmol, 95 % yield, 91% *ee*) in 35% global yield with respect to the starting racemic mixture (±)-**1**.

*2.4. Synthesis of enantiomers of 1-formyl-2-hydroxymethylferrocene, (+)-**2** and (–)-**2**.*

To a solution of (*1R_p*)-(+)-**1** (110 mg, 0.42 mmol, 94% *ee*) in CH_2Cl_2 (15 mL) activated MnO_2 (100 mg) was added and the suspension maintained under stirring at 40 °C overnight. The mixture was filtered on a Celite pad and the solution taken to dryness. The residue was purified by column chromatography (Si gel, *n*-hexane:AcOEt, 7:3) to afford *(1S_p)-1- formyl-2-methoxymethylferrocene* (+)-**4** (100 mg, 0.39 mmol, 94% yield, 94 % *ee*) as a dark orange oil whose characterization data were in agreement with those reported for the racemic compound [20]. $[\alpha]_D^{25}$ +15.8 (*c* 0.30, $CHCl_3$). HPLC: *n*-hexane:2-PrOH 75:25, t_R/min 19.58 (*1R_p*) and 23.91 (1S_p).

According the same procedure, starting from (1S_p)-(–)-**1** (140 mg, 0.54 mmol, 91% *ee*) the corresponding *(1R_p)-1-formyl-2-methoxymethylferrocene* (–)-**4** was obtained (130 mg, 0.50 mmol, 93% yield, 91% *ee*).

Aldehyde (*1S_p*)-(+)-**4** (100 mg, 0.39 mmol, 94% *ee*) was suspended in acetone/H_2O (1:1 v/v, 10 mL) and montmorillonite K-10 (100 mg) was added. The mixture was stirred at 42° C for 24 h, then filtered on a short plug of Celite washing the solid with CH_2Cl_2 (10 mL). The solution was taken to dryness and the residue purified by chromatography on silica gel using *n*-hexane: AcOEt 70:30 to afford pure *(1S_p)-1- formyl-2-hydroxymethylferrocene* (–)-**2** (45 mg, 0.18 mmol, 45%

yield, 94% *ee*) as an orange oil. $[\alpha]_D^{25}$ –262.1 (*c* 0.38, $CHCl_3$). $[\alpha]_D^{25}$ –20.8 (*c* 0.13, EtOH). Lit. [18] $[\alpha]_D^{25}$ –91.7 (*c* 0.1, EtOH, 94% *ee*). ^{1}H-NMR: δ 3.89 (br t, 1H, -OH), 4.33 (s, 5H. Cp'), 4.54 (m, 3H, 2 x CH_a-O and 2 x Cp), 4.71 (d, *J* = 12.8 Hz, 2H, 2 x CH_b-O), 9.96 (s, 1H, CHO). ^{13}C-NMR: δ 59.5 (-CH_2OH), 70.2 (Cp'), 71.6 (Cp), 73.3 (Cp), 74.9 (Cp), 77.2 (Cp-q), 90.75 (Cp-q), 196.1. HPLC: *n*-hexane:2-PrOH 75:25, t_R/min 33.92 (*1R*$_p$) and 51.52 (*1S*$_p$). HR-ESI-MS: 227.0197 [M – OH]$^+$, 267.0128 [M + Na]$^+$, 511.0364 [2M + Na]$^+$, theor. for $C_{12}H_{12}FeNaO_2$ 267.0084.

According the same procedure, starting from (*1R*$_p$)-(–)-**4** (130 mg, 0.50 mmol, 91% *ee*) the corresponding (*1R*$_p$)-*1-formyl-2-hydroxymethylferrocene* (+)-**2** was obtained (56 mg, 0.23 mmol, 46% yield, 91% *ee*).

*2.5. Synthesis of enantiomers of 1-iodo-2-hydroxymethylferrocene, (+)-**3** and (–)-**3**.*

According to a reported procedure [19], alcohol (±)-**3** (400 mg, 1.17 mmol) was dissolved in CH_2Cl_2 (50 mL) and lipase Novozym® (0.8 g) and vinyl acetate (0.6 mL, 560 mg, 6.51 mmol) were added. The suspension was stirred in a rotary shaker at 300 rpm and 45 °C for 12 h when 35% of the substrate conversion was reached. After filtration of the enzyme, the solution was taken to dryness and the residue purified on a deactivated silica gel column (*n*-hexane:AcOEt 3:1) to give (*1S*$_p$)-1-iodo-2-acetoxymethylferrocene from which (*1S*$_p$)*-1-iodo-2-hydroxymethylferrocene* (–)-**3** (116 mg, 0.34 mmol, 29% yield, 96% *ee*) was recovered after alkaline hydrolysis and recrystallization from *n*-hexane, $[\alpha]_D^{25}$ –23.8 (*c* 0.42, $CHCl_3$). A parallel reaction was carried out for 3 days after which 55% conversion of substrate was reached. After work-up as above, the unreacted (*1R*$_p$)*-1-iodo-2-hydroxymethylferrocene* (+)-**3** was isolated by column chromatography and recrystallized from *n*-hexane (145 mg, 0.42 mmol, 36% yield, 98% *ee*). $[\alpha]_D^{25}$ +23.5 (*c* 0.19, $CHCl_3$). HPLC: *n*-hexane:2-PrOH 90:10, t_R/min: 20.62 (1*S*$_p$) and 24.81 (1*R*$_p$).

The raw NMR spectra for the three compounds are given in Figures SI-1, SI-2, and SI-3; the chiral HPLC chromatograms are given in Figures SI-4, SI-5, and SI-6.

2.6. VCD spectra

VCD spectra were obtained on a Jasco FVS6000 FTIR-based instrument, equipped with a wire-grid linear polarizer and ZnSe photo-elastic modulator to generate alternatively left and right circularly polarized radiation at 50 kHz frequency, to be recorded and amplified with lock-in amplifier. Two liquid-N_2 cooled detectors were employed, an MCT-one for the mid-IR and C=O stretching region, and an InSb-one for the CH-/OH-stretching regions. For the mid-IR/C=O stretching regions 200 μm-pathlength BaF_2 cells were employed; for the other regions QX-Hellma® quartz cuvettes 1mm, 5 mm and 10 mm thick for the CH/OH-stretching regions were used. Solution concentrations were comprised between 0.15 to 0.02 M; we employed several

solvents, CS_2, CCl_4, $CDCl_3$. Results reported in the text are for CCl_4 in all regions and for all compounds, except for (±)-**1**, where we report results for the CS_2 solvent in the mid-IR region. All VCD spectra were acquired with 5000 scans and the same procedure was adopted for the solvent, whose spectrum was subtracted from that of the solution, both for the VCD and the IR-absorption spectra. Original spectra obtained in this way for both enantiomers of compounds **1**, **2** and **3** showed good mirror-image behavior and are provided in the Supplementary Material (Figures SI-8, SI-10, and SI-12), while the VCD spectra given in the text are semi-differences thereof.

2.7. ECD spectra

ECD spectra were obtained on a Jasco J815SE instrument for 0.005 M/acetonitrile solutions for all three enantiomeric pairs of **1**, **2** and **3**. The solutions were contained in Hellma quartz cuvettes, which had 0.1 mm-pathlength for the 180-280 nm region and, for the 280-600 nm region, 1 mm-pathlength for **1**, 2 mm for **2** and 1 mm for **3**. 5 scans were acquired for each enantiomer and for the solvent, whose spectrum was subtracted from the spectrum of the solution. The original spectra are provided in the Supplementary Material (Figure SI-15), while the ECD spectra given in the text are semi-differences thereof.

2.8. DFT calculations

Prior to DFT calculations, the conformational search was started by generating all conformers obtainable by rotating around sp^3 bonds, connecting the external groups to the ferrocene core through the VEGA ZZ program (force field SP4) [21]. DFT calculations were run after this step, at B3LYP/6-31G* in vacuo. Finally, retaining conformers within a 5 kcal/mol interval, DFT optimization and frequency calculations was performed at the B3PW91/def2tzvp/PCM level of theory [14-15, 22-23] with the appropriate solvent in the PCM [24] part, all modules being in Gaussian16 [25]. The further defined conformers are shown in Table 1 below and statistical Boltzmann weights based on energy or free energy were obtained and used in the next step. To properly account for the calculated ECD/UV spectra (*vide infra*), we considered the PCM approach also with CH_3CN solvent. Only small differences in population factors are found from CCl_4, as may be appreciated from Table SI-2. Rotational strength for VCD spectra were then generated through the so called Stephens' algorithm [26], based on linear response theory, to overcome the vanishing magnetic dipole transition moment paradox. The spectra were calculated at the harmonic level (both in the electrical and mechanical part), taking advantage of our previous investigations, where anharmonicity showed important but not decisive to predict VCD and IR spectra [14,15]. The IR and VCD spectra were then obtained by placing bands for each transition at the calculated wavenumber, with area equal to the calculated dipole strength or rotational strength, with a

Lorentzian band-shape having 10 cm^{-1} band-width for mid-IR and 20 cm^{-1} band-width for the CH/OH stretching regions. In order to cope with mechanical anharmonicity and to better compare with experiments, VCD spectra were shifted by the use of a scaling factor, which was 0.96 for the mid IR region and 0.955 for the CH/OH stretching regions. The calculated spectra for each conformer are shown in the Supplementary Material, while the calculated spectra in the text are Boltzmann-averages based on ΔG-weights. The TD-DFT procedure was employed to calculate rotational strengths and dipole strengths for the ECD and UV spectra, employing 100 states at the CAM-B3LYP/def2tzvp/PCM level of theory [14-15, 24] (Coulomb attenuation being sort of standard in the case of electronic properties); calculated spectra were obtained similarly to VCD spectra, with a +20 nm rigid shift and with a Gaussian waveform with σ=0.3 eV. Both in VCD and in ECD multiplicative factors in the ordinate axis are explicitly indicated, when employed.

3. Results and Discussion

3.1. Synthesis of chiral ferrocenes

Due the ability of methoxymethyl substituent to act as a *ortho*-directing group in the metalation-electrophilic quenching sequence usually employed for the synthesis of 1,2-disubstituted ferrocenes, the intermediate (±)-**4** was prepared from methoxymethylferrocene and dimethylformamide according to a reported procedure [20] and then reacted with $NaBH_4$ to give 1-methoxymethyl-2-hydroxylmethylferrocene (±)-**1** (Scheme 2).

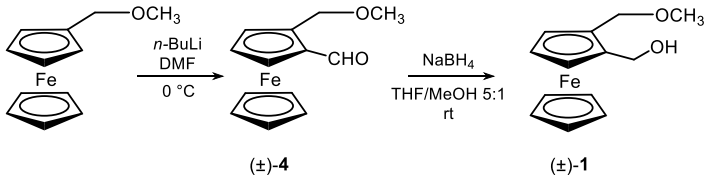

Scheme 2. Synthesis of racemic 1-methoxymethyl-2-hydroxymethylferrocene (±)-**1**

Single enantiomers of **1** were obtained from lipase-catalyzed esterification of the racemic mixture (±)-**1**, applying a protocol developed for the kinetic resolution of other 1,2-disubstituted ferrocenes possessing only planar chirality [19, 27-28]. A preliminary screening revealed that most of the tested lipases (Table SI-1) exhibited poor enantioselectivity and low reactivity, while lipase from *Pseudomonas cepacia* immobilized on ceramic (PsL-D) catalyzed the esterification of (±)-**1** with sufficient enantiodiscrimination and good reaction rate. Attempts to improve the enantioselectivity of PsL-D by changing the solvent or the acyl donor were unsuccessful, while lowering the temperature led to a sensible decrease of the reaction rate not balanced by better performance in the enzyme recognition.

So, we resorted to a two-step procedure (Scheme 3) in which the lipase-catalyzed esterification was firstly carried out on the (±)-**1** over 50% of the substrate conversion to give unreacted (+)-**1** in good optical purity (94% *ee*) and the ester product (–)-**5** in 44% *ee.* Scalemic alcohol (–)-**1**, obtained from chemical hydrolysis of (–)-**5**, was then used as substrate in a second step of biocatalyzed acetylation resulting in increased optical purity of the formed product (–)-**5** up to 91% *ee*. From the overall process both enantiomers of (+)-**1** and (–)-**1** were thus obtained in moderate yield (60 and 70% of the theoretical yield for each enantiomer) and satisfactory optical purity. The AC of (+)-**1** and (–)-**1** was assigned by chemical correlation with the known 1-formyl-2-hydroxymethylferrocene **2** (*vide infra*).

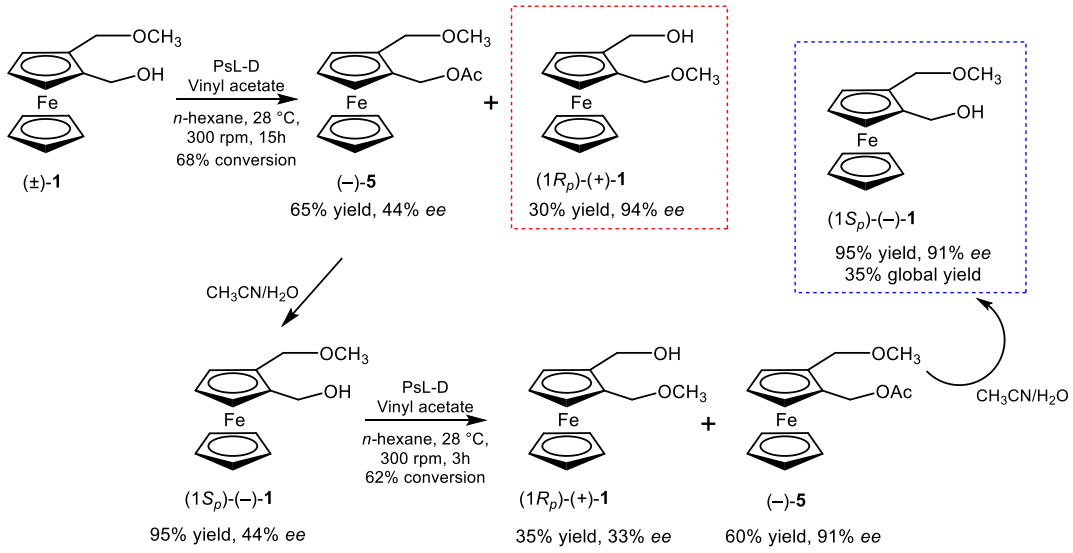

Scheme 3. Preparation of (+)-**1** and (–)-**1** by a sequence of lipase-catalyzed esterification reactions

Direct resolution of racemic 1-formyl-2-hydroxymethylferrocene (±)-**2**, obtained by demethylation of (±)-**4**, was attempted by lipase-catalyzed esterification but all the tested lipases scarcely reacted and increasing reaction temperature led to extensive degradation of the substrate.

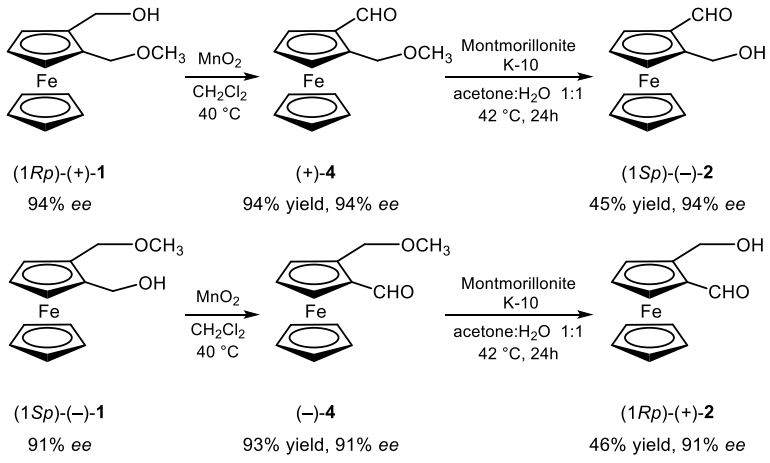

Scheme 4. Synthesis of (–)-**2** and (+)-**2** from single enantiomers of **1**

Enantiomers of **2** have been previously obtained from complementary reactions biocatalyzed by horse liver hydrogenase [18] but, needing to chemical correlate (+)-**1** to a known derivative for the assignment of its AC, we applied an alternative route for the preparation of optically active **2**.

Single enantiomers of **2** were then prepared starting from optically active (+)-**1** and (–)-**1** as in Scheme 4 using montmorillonite K-10 as acid catalyst in aqueous solvent [29]. Although in these conditions moderate yield of the target products was obtained, the use of more acidic conditions, higher reaction temperature or prolonged time led to further decreased product yield. The AC of (–)-**2** was assigned as 1S_p by comparison its sign of optical rotation with literature data [18].

Lipase-catalyzed kinetic resolution of the racemic mixture of (±)-**3** following a reported procedure [19] allowed to obtain pure enantiomers of the ferrocenyl iodoalcol.

3.2. AC assignment and study of conformational properties through chiroptical spectroscopies

3.2.1. VCD spectra

The VCD and IR absorption spectra for (+)-**1** and (–)-**1** were recorded in CS_2 and CCl_4 solvents in the mid-IR and in CCl_4 in the CH-stretching and OH-stretching regions. Results for the CS_2 solution exhibited less noisy features with better mirror image aspect for the two enantiomers in the mid-IR and the spectra in this solvent were employed in this region; to be consistent with the spectroscopic data of the other chiral ferrocenes we had previously studied, for the other two spectral regions data from the CCl_4 solutions are given in Figure 1.

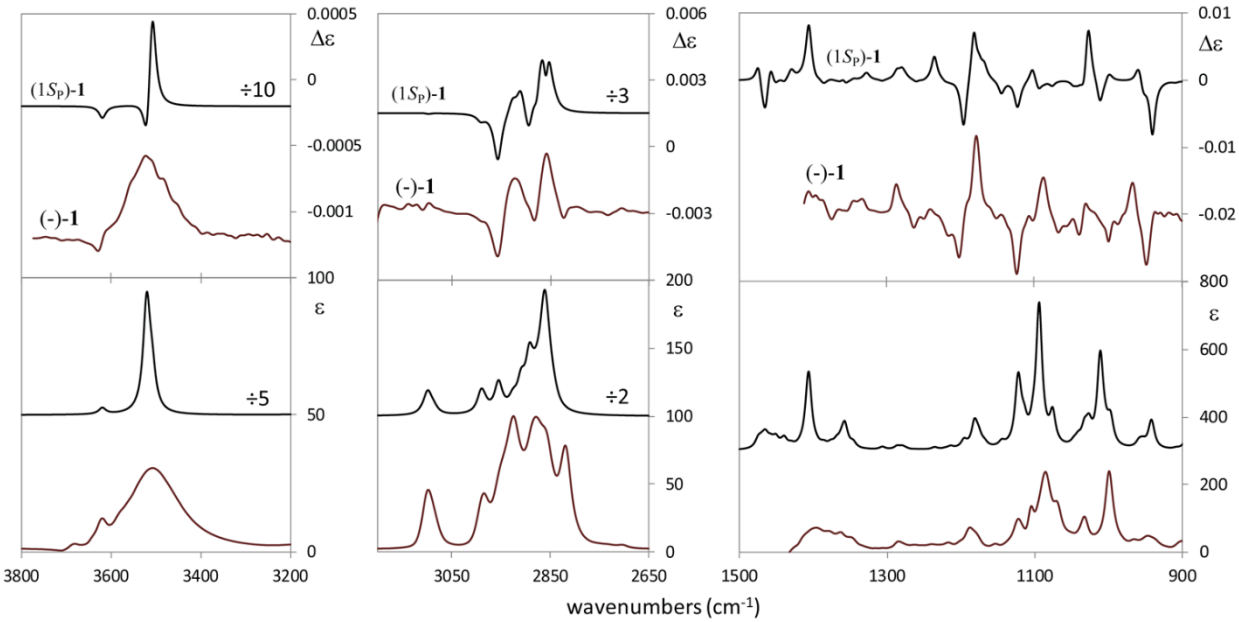

Figure 1. Comparison of experimental (red, bottom) VCD and IR spectra of (–)-**1** with the corresponding calculated spectra for (1S_p)-**1** (black, top). See details in experimental and text. Left: OH-stretching region; Center: CH-stretching region; Right: mid-IR region. Experimental VCD spectra are reported as Semi-difference. Calculated spectra were obtained at DFT/B3PW91/def2tzvp/PCM(CS_2 or CCl_4) level.

The interested reader may compare data in different solvents for both enantiomers in both solvents in Figure SI-8. In Figure 1 the experimental VCD spectra, reported as semidifference (½)[(–)-**1** – (+)-**1**], and IR absorption spectra of (–)-**1** are compared with the corresponding Boltzmann-averaged spectra of (1*S*$_p$)-**1** calculated in the suitable solvent. In Figure SI-9 calculated spectra for each conformer of (1*S*$_p$)-**1** are compared to the experimental spectra of (½)[(–)-**1** – (+)-**1**].

For compounds (+)-**2** and (–)-**2**, the VCD and IR data were acquired in CS_2, $CDCl_3$ and CCl_4 solvents in the mid-IR and in CCl_4 in the C=O-stretching, CH-stretching and OH-stretching regions. (see Figure SI-10) In this case the results for the different solvents in the mid-IR presented little differences and experimental data for (½)[(–)-**2** – (+)-**2**], given in Figure 2, were taken from CCl_4 and compared with the corresponding calculated Boltzmann averaged spectra of (1*S*$_p$)-**2**. Calculated spectra for each conformer may be consulted in Figure SI-11. A more accurate treatment with the PCM approach for different solvents would be necessary to account for the differences in Figures SI-10. But this is beyond the scopes of this work.

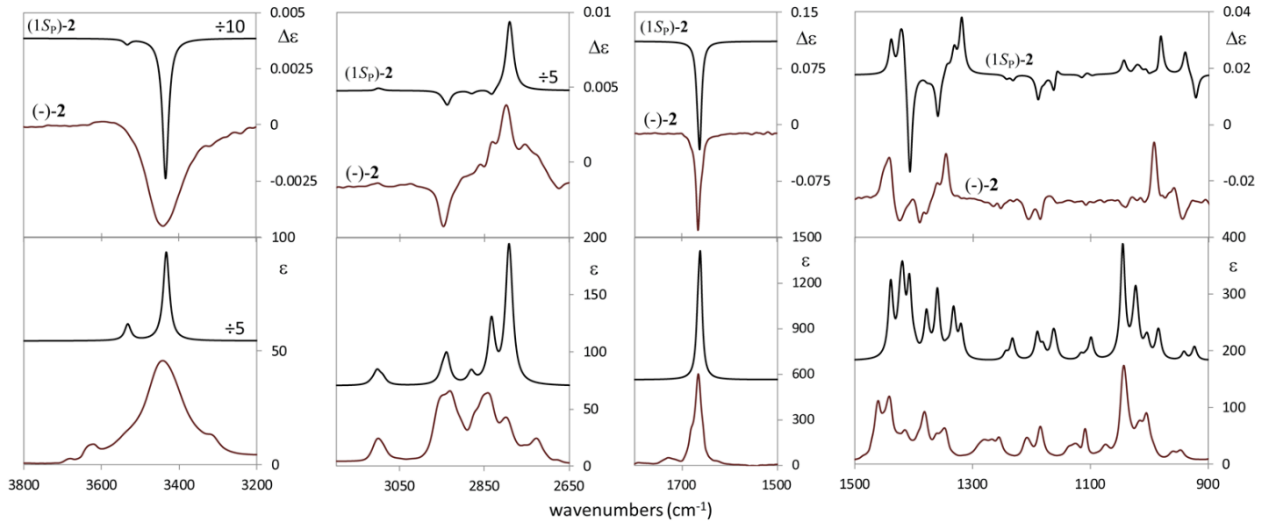

Figure 2. Comparison of experimental (red, bottom) VCD and IR spectra of (–)-**2** with the corresponding calculated spectra for (1*S*$_p$)-**2** (black, top). See details in experimental and text. Left: OH-stretching region; Center: CH-stretching region; Right: C=O + mid-IR stretching region. Experimental VCD spectra are reported as Semi-difference. Calculated spectra were obtained at DFT/B3PW91/def2tzvp/PCM(CCl_4) level.

The VCD and IR spectra of (+)-**3** and (–)-**3** were acquired just in CCl_4 (Figure SI-12) and the spectra for (½)[(–)-**3** – (+)-**3**] were compared with the corresponding calculated Boltzmann averaged spectra of (1*R*$_p$)-**3** (Figure 3). In Figure SI-13 the calculated spectra for each conformer are provided and compared to the experimental data.

For each different compound, the energetic and geometrical characteristics of the various conformers are given in Table 1 together with the 3D-representation of the calculated conformers for (1*S*$_p$)-**1**, (1*S*$_p$)-**2** and (1*R*$_p$)-**3** with population factors larger than 10%.

Populations of conformers for both (1S_p)-**1** and (1S_p)-**2** are largely affected by intramolecular HB between the -CH_2OH and the -CH_2COCH_3 and -CHO groups, respectively. In the former case we calculate just a 16.6% of non-HB conformer population, while in the latter compound both calculated conformers display HB. This has a nice counterpart in our NMR measurements which were carried out on both **1** and **2** in $CDCl_3$ at different solute concentration in the range 20-60 mM to monitor the differences in the chemical shift of the hydroxyl proton. The OH resonances were observed at δ_{OH}=2.57 ppm and δ_{OH}=3.78 ppm for **1** and **2**, respectively, and they were both found substantially unchanged upon dilution ($\Delta\delta$ = –0.018 ppm for **1** and –0.005 ppm for **2**), corroborating the predominance of intramolecular HB over intermolecular ones. Furthermore, the signal for hydroxyl proton in **2** was visible as a triplet (due to coupling with the protons of the vicinal CH_2 group), instead of a broad singlet as in **1**, suggesting a stronger HB-locked conformation in **2** compared to **1**, as also indicated by IR and VCD in the OH-stretching region (*vide infra*). In the same range of concentration, the hydroxyl resonance of **3** (δ_{OH}=1.67 ppm) was shifted upfield by 0.045 ppm. NMR spectra as function of concentration are given in Figure SI-7.

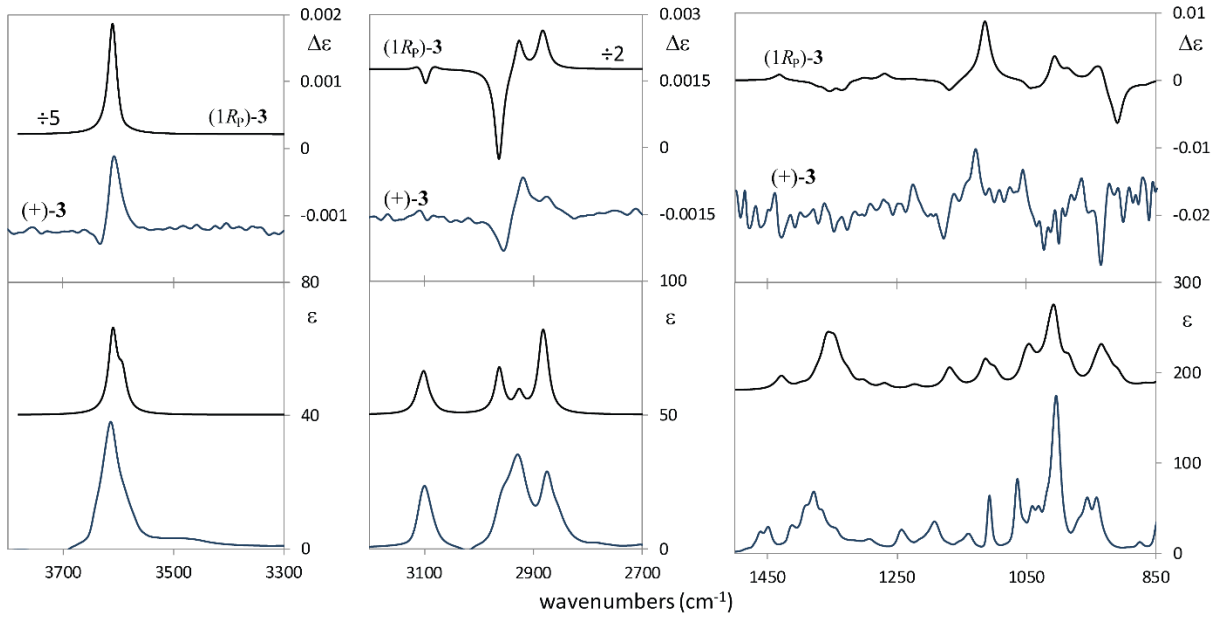

Figure 3. Comparison of experimental (red, bottom) VCD and IR spectra of (+)-**3** with the corresponding calculated spectra for (1R_p)-**3** (black, top). See details in experimental and text. Left: OH-stretching region; Center: CH-stretching region; Right: mid-IR region. Experimental VCD spectra are reported as Semi-difference. Calculated spectra were obtained at DFT/B3PW91/def2tzvp/PCM(CCl_4) level.

For compound **1,** the position of the OCH_3 group with respect to the -CH_2 group connecting it to the pentadienyl moiety, described by dihedral angle ϑ, (Table 1) may be either *trans* (ϑ = 179.9°, conformers I and III) or *gauche* (ϑ ~ 70°, conformers II and IV*)* without great influence on the ratio of the number of HB(intramolecular)-conformers to the number of non-HB(intramolecular)-conformers, which is 4.98 when the OCH_3 group is *trans*, and 5.17 when it is

gauche. In the non HB-conformers the OH is directed towards the non-vicinal pentadienyl and the iron atom.

Table 1. Energy values (ΔE and ΔG), ΔG-based population factors, selected geometrical parameters and 3D-representation for (1S_p)-**1**, (1S_p)-**2**, and (1R_p)-**3** conformers.[a]

Conformer	ΔE	ΔG	pop.%	χ	Φ	τ	ϑ	*d*	*d'*
(1S_p)-**1**									
I	0.00	0.00	65.3	0.3	–75.3	52.3	179.9	2.13	4.42
II	0.28	0.76	18.1	0.5	–72.2	58.1	70.7	2.09	4.44
III	1.88	0.96	13.1	3.5	145.5	–44.9	179.9	5.27	3.02
IV	2.30	1.73	3.5	3.1	146.4	–46.3	69.0	5.23	3.03
(1S_p)-**2**									
I	0.00	0.00	73.8	–1.5	–46.8	56.2		1.83	3.70
II	0.89	0.61	26.2	1.2	61.1	68.5		2.00	4.37
(1R_p)-**3**									
I	0.00	0.00	73.2	–0.4	88.6	–62.9		3.47	4.60
II	0.37	0.60	26.8	–4.1	–148.2	49.7		4.96	3.08

[a]Energy values in kcal/mol, angles in degrees, distances in Å. ΔG-based population factors above 10%. Calculations were run in the PCM CCl_4 approximation; also PCM CS_2 approximation was tested and found identical to CCl_4 within 2%. Geometrical parameters are: χ=H(l)-C(l)-C(u)-H(u) measuring the distortion of the above cyclopentadiene ring with respect to the ring below; Φ=C(1)-C(2)-C(ext)-O; τ=C(2)-C(ext)-O-H, ϑ=C(2)-C-O-CH3, d= -OH···O distance, d'= H-Fe distance (For **3** *d*= -OH···I distance). 3D-structures calculated via DFT for the most populated conformers of (1S_p)-**1** (top), (1S_p)-**2** (center) and (1R_p)-**3** (bottom) are shown below.

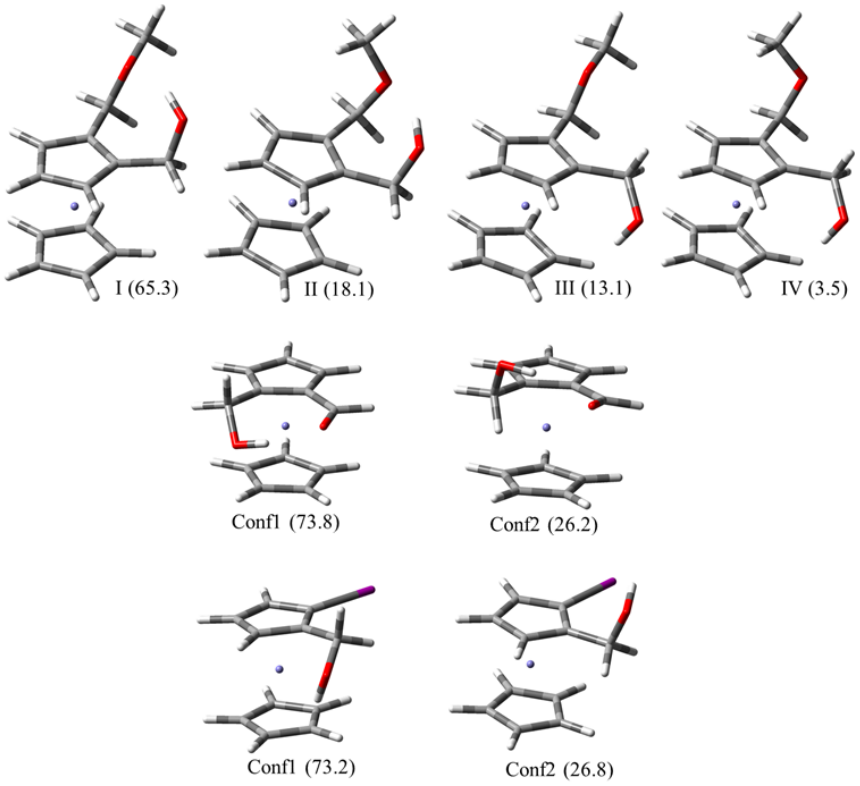

The two predicted conformers of **2** account for two arrangements of the CH_2OH group, which entertains HB with the CHO group in both situations. Lastly, in the most populated conformer of **3** the OH group is directed towards the iodine atom and thus interacts through a modest HB with it. Though the OH-stretching frequency is almost the same as that found in mono substituted chiral ferrocenes, which we had previously studied, i.e. ~ 3610 cm^{-1} [14].

For that concerns calculated VCD and IR spectra, we decided in this study to resort to the harmonic B3PW91/DEF2TZVP approach rather than the more complete anharmonic VPT2/GVPT2 model employed in our previous work on ferrocenylalcohols with central chirality [14], since good performance of the harmonic approximation had been verified also on ferrocene derivatives possessing both planar and central chirality [15].

Although less complete, the harmonic approximation was undertaken and found acceptable on a heuristic basis in this case. Indeed, it is well known that anharmonicity is most important to obtain the correct frequencies and spectral shape, especially in the CH-stretching region, where a more complete treatment is necessary [14, 30]. In the case in hand, adjusting the wavenumber difference through the use of a scaling factor [22-23, 31] appropriate to each region (see Materials and Methods section), was sufficient to obtain excellent performance of calculated VCD spectra when compared with experimental spectra (Figures 1-3) in all the investigated spectroscopic regions of all the three compounds.

On the basis of the comparison of experimental and calculated spectra, the assignment of absolute configuration, previously assessed by chemical correlation methods, was confirmed for all the tested compounds.

Looking more closely at the VCD spectra of Figures 1-3, we also may comment that while DFT calculations guarantee the proposed AC assignment, it is hard to find specific signals as markers of the planar AC, as had been done e.g. in ref. [32] where a triplet of VCD bands with alternating signs was identified to correlate with *p*-cyclophane planar chirality.

First, comparing the experimental VCD spectra in the various regions in the three compounds a common feature was found in the presence of a (–,+) doublet (from low to high wavenumbers) visible at 940 and 963 cm^{-1} for (–)-**1**, at 940 and 955 cm^{-1} for (–)-**2**, at 938 and 968 cm^{-1} for (+)-**3** corresponding in all the cases to IR doublets. Also calculations match the observed spectra: we verified that this band corresponds to a combination of CH_2-wagging and OH-bending modes in the CH_2OH group coupled with in-plane CH bending of the cyclopentadienyl ring carrying the substituents. These normal modes are more or less constant in the three compounds and can be associated to the spatial disposition of hydroxymethyl group, which is flanked on its left side by the other substituent in all these three stereoisomers and has the same $2R_p$ configuration. The opposite

(1R_p) AC of (+)-**3** with respect to (–)-**1** and (–)-**2** results from the formal application of the C.I.P. priority rules [17, 33] rather than to the different spatial orientation of the substituents on the cyclopentadienyl ring, taking into account also the presence of the Fe atom. A similar situation in which the spatial group disposition dictates the VCD response in the CH-stretching region, independently on priority rules, had been observed and explained for (1*R*)-fenchone and (1*S*)-camphor and related molecules [34].

Furthermore, the spectra in the CH-stretching region show a negative band at ca. 2950 cm^{-1} for all three compounds, corresponding to the CH_2-antisymmetric stretching normal mode in the CH_2OH group and an overall positive multiplet of VCD bands in the 2930-2800 cm^{-1} range. In the latter region, which contains symmetric CH_2/CH_3 stretching normal modes, the anharmonic phenomenon of Fermi resonance with overtones/combinations of CH_2-bendings, not treated here, should permit a more detailed explanation of the bands [35]. Both these signals have the same relevance for planar AC as the (–,+) doublet in the low wavenumber region.

Undoubtedly, though, the most interesting feature in (–)-**2** is the isolated C=O stretching band, which has strong and negative VCD (its *g* factor is between 10^{-4} and 10^{-3}, while in the rest of the spectra for (–)-**2** and for all the other compounds *g* is between 10^{-5} and 10^{-4}), in this differing from the not generally intense VCD bands exhibited by most of ketones with just one C=O bond [36]. Indeed, when two interacting C=O stretchings are present, one has been able to observe strong C=O VCD couplets associated to vibrational excitons [37-39] and, in few cases, monosignated bands associated with isolated C=O [40]. This VCD band in molecule (–)-**2** is influenced by intramolecular HB and, according to the calculations, the same sign is predicted for both conformers of (1S_p)-**2**: being insensitive to conformation, this band could have some diagnostic value for assigning AC and we think it is more informative about molecular interactions than about AC.

Other interesting features appear in the OH-stretching region: the IR spectrum of (–)-**1** shows a major absorption band at 3500 cm^{-1} and two shoulders at 3612 and 3673 cm^{-1}; for (–)-**2** the strongest IR absorption band is found at 3432 cm^{-1} with two shoulders at 3617 and 3675 cm^{-1} (a third shoulder is observed at 3309 cm^{-1}) whereas for (+)-**3** there just one absorption band at 3610 cm^{-1}. Correspondingly in the VCD spectrum of (–)-**1** there are a major positive band at 3513 cm^{-1} and a minor negative band at 3625 cm^{-1}; in (–)-**2** there is just a major negative band at 3431 cm^{-1}; in (+)-**3** there are a positive band at 3604 cm^{-1} and a weak negative shoulder at 3631 cm^{-1}.

The major IR and VCD absorption bands in **1** and **2**, hence, are sensibly shifted at lower wavenumber compared to **3**, as a consequence of a major influence of intramolecular HB in the

former compounds, whereas the minor bands around 3610 and 3670 cm^{-1} could be ascribed to the OH-stretching mode resulting from almost free OH-stretching vibration, which is predominant in **3**.

A more detailed analysis of the calculated VCD spectra of the single conformers of alcohol (1S_p)-**1** revealed that conformers III and IV, which lack intramolecular HB, display only a negative band around 3600 cm^{-1}, while conformers I and II give a band around 3430 cm^{-1} and exhibit intramolecular HB with markedly larger intensity even though with opposite sign and, suggesting a role of the –OMe orientation. The band centered at about 3600 cm^{-1} observed for (+)-**3** is correctly predicted in sign and intensity for the two calculated conformers of (1R_p)-**3,** with no influence from HB.

The calculated VCD spectra of both conformers of **2** show a negative band, with large difference in intensity and slight difference in wavenumber (around 3450 cm^{-1}), as determined by HB in both cases. The –OH-stretching major band thus does not appear as diagnostic for the assignment of AC, and the opposite sign observed for **1** and **2** in VCD spectra is not amenable to a simple interpretation, though being matched by DFT calculations: the strong perturbation from intramolecular HB is responsible for this. On the other hand, the sign of non-HB VCD calculated spectra (conformers III and IV) is negative for (1S_p)-**1** and positive for (1R_p)-**3**. However, since this band looks structured and wavy in the spectrum of **1**, we changed a bit the angle for τ (Cp-C-O-H) in Table 1 off equilibrium by 15° for the two most populated conformers I and II and the obtained calculated VCD spectra (Figure SI-14) showed that a sign change is possible in this case for conformer I, thus proving that the mobility of the OH bond may strongly influence the band-shape of the VCD band, which we surmise be also solvent-dependent.

This is a further reason why the major band in this region for compounds **1** and **2** is less relevant for empirical determination of AC, although the OH-stretching region has considerable value from the conformational point of view and HB properties.

3.2.2. ECD spectra

The ECD analyses of separate enantiomers of **1**, **2** and **3** were carried out in CH_3CN solution and the experimental spectra showed excellent overall correspondence with calculated data, as can be viewed in Figure 4 (the UV data, together with the original ECD spectra for the independent enantiomers are given in Figure SI-15).

The ECD spectra can be divided into two regions, each one exhibiting overall similar bands with the same sign and approximately one order of magnitude different in intensity for all the three molecules. The first region, ranging from 600 to ca. 300 nm, for (–)-**1** comprises a negative band at 489 nm and two positive bands at 420 and 339 nm; for (–)-**2** it comprises a negative band at 500

nm, a positive band at 377 nm and a negative one at 343 nm; finally, for (+)-**3** it comprises a negative band at 491 nm and a positive one at 324 nm. The longest wavelength ECD band exhibits a common behavior, namely it is first negative and then positive from long to short wavelengths. Its behavior is well predicted for (–)-**2** and (+)-**3**, but not for (–)-**1**. It is associated to transitions involving the iron atom and results from the convolution of four metal-to-ligands transitions, which are ECD-active mainly due to the Cp-substitutions and is made up of a multiplicity of transitions which are also conformer dependent, a fact making its prediction difficult as noticed earlier [14,15].

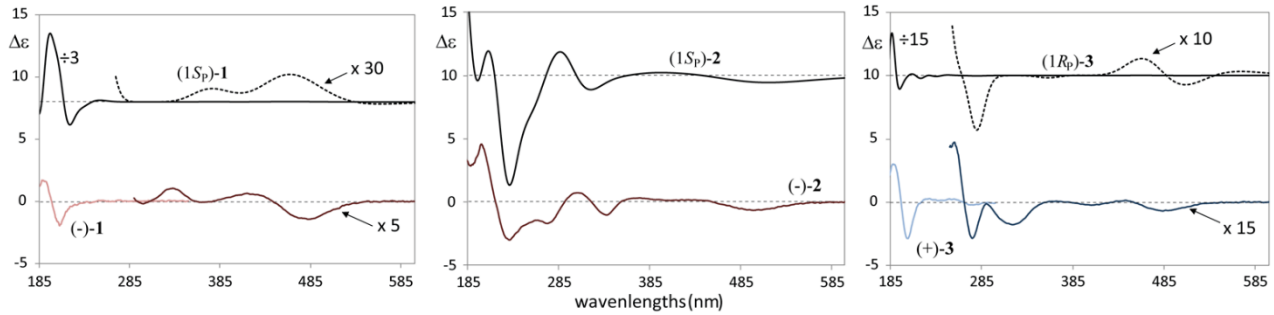

Figure 4. Comparison of experimental ECD spectra of (–)-**1**, (–)-**2**, and (+)-**3** (red, lower) with the corresponding calculated spectra of (1S_p)-**1** (left), (1S_p)-**2** (center), and (1R_p)-**3** (right) (black, higher). Experimental spectra are semi-differences of original data for (–)-**1** and (+)-**1**, of (–)-**2** and (+)-**2**, and of (+)-**3** and (–)-**3**. Calculated spectra are obtained at TDDFT/B3PW91/def2tzvp/PCM(CH_3CN) level.

The second region, ranging from 300 to 180 nm, for (–)-**1** comprises a negative-positive feature (in order of decreasing wavelength) at 210 and 195 nm, which for (–)-**2** is found at 236 and 200 nm and for (+)-**3** is at 208 and 195 nm. These transitions are π→π* ones, resident in the pentadienyl moiety distorted by the substituents providing planar chirality. While in (–)-**1** there are no other bands in the latter region, in (–)-**2** they are accompanied by other features associated to the n→π* transition of the C=O moiety. Notwithstanding this perturbation, shape and intensity of this ECD couplet is fairly constant and thus it may be useful for immediate assignment of the relative spatial disposition of substituent groups; only when perturbations from substituents are overwhelming, as in ref. [15], this nice couplet may be lost.

The same features and sign observed for the band around 500 nm and the couplet around 200 nm in (–)-**1**, (–)-**2** and (+)-**3**, seem to support the fact that the chiroptical response is dictated by the mutual spatial disposition of substituents, i.e the hydroxymethyl group on the right side of the other substituent, irrespective of the chirality descriptors, which depend on the priority rules. We point out that Pulm et al. [41] already discussed in the same way the ECD spectra of (1*R*)-fenchone and (1*S*)-camphor, which exhibit the same sign in the n→π* transition, irrespective of the absolute configuration (*vide supra* the VCD case).

It may also be noted that the longest wavelength ECD band is negative for (–)-**1**, (–)-**2** and (+)-**3** and it has the same sign as the OR value measured at 589 nm for the first two compounds, while

in the last case it is opposite. This fact is at odds with the approximate interpretation of the Kronig-Kramers relationship [42-44], on the basis of which the same sign for OR and the longest wavelength ECD band is expected, however exceptions to this rule are known for other ferrocenes [12, 45].

4. Conclusion

In this work we have recorded and discussed the VCD and ECD chiroptical spectra of three 1,2-substituted ferrocene chiral derivatives, i.e. 1-methoxymethyl-2-hydroxymethylferrocene **1**, 1-formyl-2-hydroxymethylferrocene **2** and 1-iodo-2-hydroxymethylferrocene **3**, sharing the common hydroxymethyl substituent. The combined use of VCD and ECD with DFT and TD-DFT calculations allowed unambiguous AC assignment of each compound and (–)-**1** corresponds to (1*S*$_p$)-**1**, (–)-**2** corresponds to (1*S*$_p$)-**2** and (+)-**3** corresponds to (1*R*$_p$)-**3**. Furthermore, empirically selected features in the VCD or ECD spectra, like the bisignate VCD couplet at 940, 960 cm^{-1} or the 210, 195 nm ECD couplet, were found related to the mutual disposition of the substituents independently on the AC descriptors, which are defined by the priority rules, a condition already noticed in the chiroptical literature.

Finally, it is worth to remark that several VCD features appear to be largely influenced by local characteristics, mainly related to the intramolecular HB entertained by the hydroxymethyl group (having different strength in the three compounds, between the hydroxyl and the nearby groups). In any case the DFT calculations provided full account of all observed phenomena, from the overall AC assignment to most if not all local effects.

ACKNOWLEDGEMENTS

This research has been carried out with the support of resources of Big&Open Data Innovation Laboratory (BODaI-Lab), University of Brescia, granted by Fondazione Cariplo and Regione Lombardia and of Computing Center CINECA (Bologna), Italy. Funding from the Italian Ministry of Education, University and Research (MIUR) through the PRIN 2017 program (Project 2017A4XRCA_003 “Physico-chemical Heuristic Approaches: Nanoscale Theory of Molecular Spectroscopy [PHANTOMS]”) is acknowledged.

SUPPLEMENTARY INFORMATION

Lipase screening for the biocatalyzed kinetic resolution. Experimental VCD spectra of enantiomers in different solvents. Comparison of experimental VCD and IR spectra for the investigated compounds with the calculated spectra of the different conformers predicted through DFT calculations. (O)H chemical shifts in NMR spectra of investigated compounds in $CDCl_3$ as function

of concentration. Calculated spectra in the OH-stretching region of ($1S_p$)-**1** and for ($1S_p$)-**2** for various values of dihedral angle CCOH about equilibrium. Experimental ECD spectra of enantiomers of investigated compounds.

REFERENCES

[1] L. Cunningham, A. Benson, P.J. Guiry, Recent developments in the synthesis and applications of chiral ferrocene ligands and organocatalysts in asymmetric catalysis, Org. Biomol. Chem. 18 (2020) 9329-9370. https://doi.org/10.1039/D0OB01933J.

[2] A. Khan, L. Wang, H. Yu, M. Haroon, R. S. Ullah, A. Nazir, T. Elshaarani, M. Usman, S. Fahad, F. Haq, Research advances in the synthesis and applications of ferrocene-based electro and photo responsive materials, Appl. Organomet. Chem. 32 (2018) e4575. https://doi.org/10.1002/aoc.4575.

[3] Z. Huang, H. Yua, L. Wang, X. Liu, T. Lin, F. Haq, S. Z. Vatsadze, D. A. Lemenovskiy, Ferrocene-contained metal organic frameworks: From synthesis to applications, Coord. Chem. Rev. 430 (2021) 213737. https://doi.org/10.1016/j.ccr.2020.213737.

[4] A. Singh, I. Lumb, V. Mehrac, V. Kumar, Ferrocene-appended pharmacophores: an exciting approach for modulating the biological potential of organic scaffolds Dalton Trans. 48 (2019) 2840–2860. https://doi.org/10.1039/c8dt03440k.

[5] R. Wang, H. Chen, W. Yan, M. Zheng, T. Zhang, Y. Zhang, Ferrocene-containing hybrids as potential anticancer agents: Current developments, mechanisms of action and structure-activity relationships, Eur. J. Med. Chem. 190 (2020) 112109. https://doi.org/10.1016/j.ejmech.2020.112109.

[6] J. Xiao, Z. Sun, F. Kong, F. Gao, Current scenario of ferrocene-containing hybrids for antimalarial activity, Eur. J. Med. Chem. 185 (2020) 111791. https://doi.org/10.1016/j.ejmech.2019.111791.

[7] G. Angelici, M. Gòrecki, G. Pescitelli, N. Zanna, M. Monari, C. Tomasini, Synthesis and structure analysis of ferrocene-containing pseudopeptides, Pept. Sci. 110 (2018) e23072. https://doi.org/10.1002/bip.23072.

[8] M. Nuskol, P. Šutalo, M. Đaković, M. Kovačević, I. Kodrin, M. Čakić Semenčić, Testing the Potential of the Ferrocene Chromophore as a Circular Dichroism Probe for the Assignment of the Screw-Sense Preference of Tripeptides, Organometallics 40 (2021) 1351–1362. https://doi.org/10.1021/acs.organomet.1c00138.

[9] A. Ueno, Q. Chen, I. Suzuki, T. Osa, Detection of organic compounds by guest-responsive circular dichroism variations of ferrocene-appended cyclodextrins, Anal. Chem. 64 (1992), 15, 1650–1655. https://doi.org/10.1021/ac00039a005.

[10] V. I. Sokolov, N. S. Khrushcheva, K. K. Babievsky, I. A. Yamskov, Synthesis and circular dichroism of the optically active dendrimers with the planar chiral ferrocene core, Russ. Chem. Bull. 58 (2009) 1855–1857. https://doi.org/10.1007/s11172-009-0253-6.

[11] T. Sotani, H. Iwakiri, H. Yamada, N. Shimosaraya,Y. Miyagi, F. Sanda, Synthesis, Chiroptical, and Redox Properties of Ferrocene-Containing Optically Active Polymers, Macromol. Mater. Eng. 304 (2019) 1900282. https://doi.org/10.1002/mame.201900282.

[12] I. Janowska, J. Zakrzewski, Circular dichroism spectra of planar chiral 2-substituted ferrocenecarboxaldehydes and 2-ferrocenyl-1,1-dicyanoethylenes, Tetrahedron: Asymmetry, 14 (2003) 3271-3273. https://doi.org/10.1016/j.tetasy.2003.09.005.

[13] A. Urbano, A. M. del Hoyo, A. Martínez-Carrión, M. C. Carreño, Asymmetric Synthesis and Chiroptical Properties of Enantiopure Helical Ferrocenes, Org. Lett. 21 (2019) 4623–4627. https://doi.org/10.1021/acs.orglett.9b01522.

[14] A. Patti, S. Pedotti, G. Mazzeo, G. Longhi, S. Abbate, L. Paoloni, J. Bloino, S. Rampino, V. Barone, Ferrocenes with simple chiral substituents: an in-depth theoretical and experimental VCD and ECD study, Phys. Chem. Chem. Phys. 21(2019), 9419-9432. https://doi.org/10.1039/C9CP00437H.

[15] M. Ravutsov, G. M. Dobrikov, M. Dangalov, R. Nikolova, V. Dimitrov, G. Mazzeo, G. Longhi, S. Abbate, L. Paoloni, M. Fusè, V. Barone, 1,2-Disubstituted Planar Chiral Ferrocene Derivatives from Sulfonamide-Directed ortho-Lithiation: Synthesis, Absolute Configuration, and Chiroptical Properties, Organometallics 40 (2021) 578−590. https://doi.org/10.1021/acs.organomet.0c00712.

[16] S. R. Domingos, H. J. Sanders, F. Hartl, W. J. Buma, S. Woutersen, Switchable Amplification of Vibrational Circular Dichroism as a Probe of Local Chiral Structure, Angew. Chem., Int. Ed. 53 (2014) 14042–14045. https://doi.org/10.1002/ange.201407376.

[17] R. S. Cahn, C. K. Ingold, V. Prelog, Specification of Molecular Chirality, Angew. Chem. Int. Ed. Engl. 5 (1966) 385-415. https://doi.org/10.1002/anie.196603851.

[18] Y. Yamazaki, K. Hosono, Stereoselectivity of horse liver alcohol dehydrogenase catalyzed oxidoreduction of an organometallic meso diol and the corresponding dialdehyde, Tetrahedron Lett. 29 (1988) 5769-5770. https://doi.org/10.1016/S0040-4039(00)82187-5

[19] A. Patti, D. Lambusta, M. Piattelli, G. Nicolosi, Lipase-mediated resolution of 2-hydroxymethyl-1-iodoferrocene: synthesis of ferrocenes and biferrocenes with planar chirality, Tetrahedron: Asymmetry 9 (1998) 3073–3080. https://doi.org/10.1016/S0957-4166(98)00311-5.

[20] O. Delacroix, B. Andriamihaja, S. Picart-Goetheluck, J. Brocard, About diastereoselective oxidations of ferrocenyl amino alcohols, Tetrahedron 60 (2004) 1549–1556. https://doi.org/10.1016/j.tet.2003.12.004.

[21] A. Pedretti, A. Mazzolari, S. Gervasoni, L. Fumagalli, G. Vistoli. The Vega Suite Of Programs: An Versatile Platform For Cheminformatics And Drug Design Projects. Bioinformatics, 37 (2021) 1174-1175. https://doi.org/10.1093/bioinformatics/btaa774.

[22] P.L. Polavarapu, “Chiroptical Spectroscopy Fundamentals and Applications” CRC Press (Taylor & Francis Group), 2019, Baton Rouge, LA, USA.

[23] P.J. Stephens, F.J. Devlin, J.R. Cheeseman, “VCD Spectroscopy for Organic Chemists” CRC Press (Taylor & Francis Group), 2019, Baton Rouge, LA, USA.

[24] J. Tomasi, B. Mennucci, R. Cammi, Quantum Mechanical Continuum Solvation Models, Chem. Rev. 105 (2005) 2999–3094. https://doi.org/10.1021/cr9904009.

[25] Gaussian 16, Revision C.01, M. J. Frisch, G. W. Trucks, H. B. Schlegel, G. E. Scuseria, M. A. Robb, J. R. Cheeseman, G. Scalmani, V. Barone, G. A. Petersson, H. Nakatsuji, X. Li, M. Caricato, A. V. Marenich, J. Bloino, B. G. Janesko, R. Gomperts, B. Mennucci, H. P. Hratchian, J. V. Ortiz, A. F. Izmaylov, J. L. Sonnenberg, D. Williams-Young, F. Ding, F. Lipparini, F. Egidi, J. Goings, B. Peng, A. Petrone, T. Henderson, D. Ranasinghe, V. G. Zakrzewski, J. Gao, N. Rega, G. Zheng, W. Liang, M. Hada, M. Ehara, K. Toyota, R. Fukuda, J. Hasegawa, M. Ishida, T. Nakajima, Y. Honda, O. Kitao, H. Nakai, T. Vreven, K. Throssell, J. A. Montgomery, Jr., J. E. Peralta, F. Ogliaro, M. J. Bearpark, J. J. Heyd, E. N. Brothers, K. N. Kudin, V. N. Staroverov, T. A. Keith, R. Kobayashi, J. Normand, K. Raghavachari, A. P.

Rendell, J. C. Burant, S. S. Iyengar, J. Tomasi, M. Cossi, J. M. Millam, M. Klene, C. Adamo, R. Cammi, J. W. Ochterski, R. L. Martin, K. Morokuma, O. Farkas, J. B. Foresman, and D. J. Fox, Gaussian, Inc., Wallingford CT, 2016.

[26] P. J. Stephens, Theory of Vibrational Circular Dichroism, J. Phys. Chem. 89 (1985) 748–752. https://doi.org/10.1021/j100251a006.

[27] G. Nicolosi, A. Patti, R. Morrone, M. Piattelli, Enzyme-promoted Kinetic Resolution of 1-Hydroxymethyl-2-dimethylaminomethylferrocene, Tetrahedron: Asymmetry 5 (1994) 1275-1280. https://doi.org/10.1016/0957-4166(94)80169-X.

[28] A. Patti, D. Lambusta, M. Piattelli, G. Nicolosi, P. McArdle, D. Cunningham, M. Walsh, Lipase-assisted Preparation of Enantiopure Ferrocenyl Sulfides Possessing Planar Chirality and their Use in the Synthesis of Chiral Sulfoxides, Tetrahedron 53 (1997) 1361-1368. https://doi.org/10.1016/S0040-4020(96)01048-4.

[29] S. Pedotti, A. Patti Mild hydrolytic cleavage of α-ferrocenylalkyl-*O*-methyl ethers, Tetrahedron 68 (2012) 3300-3305. https://doi.org/10.1016/j.tet.2012.02.074.

[30] L. Paoloni, G. Mazzeo, G. Longhi, S. Abbate, M. Fusè, J. Bloino, V. Barone Toward Fully Unsupervised Anharmonic Computations Complementing Experiment for Robust and Reliable Assignment and Interpretation of IR and VCD Spectra from Mid-IR to NIR: The Case of 2,3-Butanediol and trans-1,2-Cyclohexanediol, J. Phys. Chem. A 124 (2020) 1011-1024, https://doi.org/10.1021/acs.jpca.9b11025

[31] L.A. Nafie, Vibrational Optical Activity: Principles and Applications, John Wiley & Sons, Ltd, New York, 2011.

[32] G. Mazzeo, G. Longhi, S. Abbate, F. Buonerba, R. Ruzziconi, Chiroptical Signatures of Planar and Central Chirality in [2]Paracyclo[2](5,8)quinolinophane Derivatives, Eur. J. Org. Chem. (2014) 7353-7363. https://doi.org/10.1002/ejoc.201402945

[33] S. Arae, M. Ogasawara. Catalytic asymmetric synthesis of planar-chiral transition-metal complexes. Tetrahedron Lett. 56 (2015) 1751-1761. https://doi.org/10.1016/telet.2015.01.130

[34] G. Longhi, S. Abbate R. Gangemi, E. Giorgio, C. Rosini. Fenchone, camphor, 2-Methylenefenchone and 2-Methylenecamphor: A Vibrational Circular Dichroism Study, J. Phys. Chem. A 110 (2006) 4958-4968, http://doi.org/10.1021/jp0571

[35] S. Abbate, E. Castiglioni, F. Gangemi, R. Gangemi, G. Longhi, R. Ruzziconi, S. Spizzichino, Harmonic and Anharmonic Features of IR and NIR Absorption and VCD Spectra of Chiral 4-X-[2.2]Paracyclophanes, J. Phys. Chem. A 111 (2007) 7031-7040. https://doi.org/10.1021/jp072115w.

[36] C. Guo, R. D. Shah, R. K. Dukor, T. B. Freedman, X. Cao, L. A. Nafie, Fourier transform vibrational circular dichroism from 800 to 10,000 cm^{-1}: near-ir VCD spectral standards for terpenes and related molecules. Vibr Spectrosc 42 (2006) 254–272. https://doi.org/10.1016/j.vibspec.2006.05.013.

[37] T. Taniguchi, K. Monde, Exciton Chirality Method in Vibrational Circular Dichroism, J. Am. Chem. Soc. 134 (2012) 3695–3698. https://doi.org/10.1021/ja3001584.

[38] S. Abbate, G. Mazzeo, S. Meneghini, G. Longhi, S.E. Boiadjiev, D. A. Lightner, Bicamphor: a prototypic molecular system to investigate vibrational excitons, J. Phys. Chem. A 119 (2015) 4261-4267. https://doi.org/10.1021/acs.jpca.5b02332.

[39] G. Mazzeo, E. Santoro, S. Abbate, C. Zonta, F. Fabris, G. Longhi, Testing the vibrational exciton and the local mode models on the instructive cases of dicarvone, dipinocarvone,

anddimenthol vibrational circular dichroism spectra, Chirality 32 (2020) 907–921. https://doi.org/10.1002/chir.23232.

[40] D. Rossi, R. Nasti, S. Collina, G. Mazzeo, S. Ghidinelli, G. Longhi, M. Memo, S. Abbate, The role of chirality in a set of key intermediates of pharmaceutical interest, 3-aryl-substituted-γ-butyrolactones, evidenced by chiral HPLC separation and by chiroptical spectroscopies, J. Pharm. Biomed. Anal. 144 (2017) 41-51. https://doi.org/10.1016/j.jpba.2017.01.007.

[41] F. Pulm, J. Schramm, J. Hormes, S. Grimme, S.D. Peyerimhoff. Theoretical and experimental investigations of the electronic circular dichroism and absorption spectra of bicyclic ketones. Chem. Phys. 224 (1997) 143-155. https://doi.org/10.1016/S0301-0104(97)00258-9

[42] E. Giorgio, R. G. Viglione, R. Zanasi, C. Rosini, Ab Initio Calculation of Optical Rotatory Dispersion (ORD) Curves: A Simple and Reliable Approach to the Assignment of the Molecular Absolute Configuration, J. Am. Chem. Soc. 126 (2004) 12968–12976. https://doi.org/10.1021/ja046875l.

[43] P.L. Polavarapu, Kramers−Kronig Transformation for Optical Rotatory Dispersion Studies, J. Phys. Chem. A 109 (2005) 7013–7023. https://doi.org/10.1021/jp0524328.

[44] A. Moscowitz Some applications of the Kronig-Kramers Theorem to Optical Activity, Tetrahedron, 13 (1961) 48-54. https://doi.org/10.1016/S0040-4020(01)92204-5

[45] I. Fleischer; Š. Toma Synthesis of new chiral 1,2-disubstituted ferrocenes, Collect. Czech. Chem. Commun. 2004, 69, 330-338. https://doi.org/10.1135/cccc20040330